Applied Catalysis B: Environmental 184 (2016) 142–152

Contents lists available at ScienceDirect

Applied Catalysis B: Environmental

journal homepage: www.elsevier.com/locate/apcatb

Steam reforming of hydrocarbons from biomass-derived syngas over $MgAl_2O_4$-supported transition metals and bimetallic IrNi catalysts

Vanessa Lebarbier Dagle[a], Robert Dagle[a,*], Libor Kovarik[b], Arda Genc[c], Yang-Gang Wang[a], Mark Bowden[b], Haiying Wan[a], Matthew Flake[a], Vassiliki-Alexandra Glezakou[a], David L. King[a], Roger Rousseau[a,*]

[a] Institute for Integrated Catalysis, Pacific Northwest National Laboratory, Richland, WA 99352, USA
[b] Environmental Molecular Sciences Laboratory, Pacific Northwest National Laboratory, Richland, WA 99354, USA
[c] FEI Company, 5350 NE Dawson Creek Drive, Hillsboro, OR 97124, USA

ARTICLE INFO

Article history:
Received 7 August 2015
Received in revised form
13 November 2015
Accepted 17 November 2015
Available online 25 November 2015

Keywords:
Biomass
Tar
Steam reforming
Gasification
Syngas
Ir
Rh
Ni
Bimetallic catalyst
Noble metals

ABSTRACT

This study presents an investigation into the steam reforming of hydrocarbons from biomass gasifier-derived syngas over $MgAl_2O_4$-supported transition metals (Ni, Rh, Ir, Ru, Pt, and Pd) and novel bimetallic IrNi catalysts. Using a model syngas consisting of H_2, CO, CO_2, CH_4, C_2H_4, and H_2O, Ir and Rh catalysts were found to be the most stable catalysts (at 850 °C, 1 bar, 114,000 h^{-1}). When benzene and naphthalene are added to the feed (as a tar simulant) stability is affected by both tar concentration and type of tar. Catalytic deactivation, caused primarily by coking can be minimized by operating at a high reaction temperature (e.g., 850 °C). In addition, promoting Ni catalyst with Ir significantly enhances stability. By using bimetallic formulations of Ir and Ni (0.5–5.0% Ir, 15%Ni), nickel sintering during the reaction is reduced. Surprisingly, IrNi catalysts also offer more stability than catalysts with Ir particles alone. In agreement with theoretical calculations, small Ir° clusters (~2–3 atoms) supported on large Ni° particles (≥5 nm) present more resistance to coking than either small Ir° clusters or Ni° particles alone. Hence, superior stability of the bimetallic catalysts results from both resistance to coking and a decrease in nickel sintering. Minimal loss of activity of 12% for TOS = 80 h is demonstrated for a bimetallic catalyst with optimal concentrations of 2.5% Ir and 15% Ni. Both monometallic Ir and Ni catalysts suffer substantial loss of activity (i.e., ≥40% loss, TOS = 80 h) under comparable conditions.

Published by Elsevier B.V.

1. Introduction

Biomass-derived synthesis gas (syngas) for catalytic conversion to fuels and chemicals has been the focus of much research [1]. Biomass-derived syngas must be treated to remove a number of impurities that would otherwise poison the processing catalysts. The product gas from a biomass gasifier is mainly composed of H_2, CO, CO_2, CH_4, H_2O, and small quantities of higher hydrocarbon gases such as ethane, organic compounds broadly classified as tars, and inorganic impurities, such as H_2S, HCl, NH_3, and alkali metals [2]. Many of these inorganic constituents must be removed to part per billion levels because they strongly interact with downstream water-gas-shift and/or synthesis catalysts [3]. Tars are notorious for condensing and subsequently polymerizing on downstream equipment such as compressor and gas turbine surfaces [4]. Tars and other hydrocarbons also contribute to significant carbon deposition on downstream synthesis catalyst surfaces. Catalytic reforming of the tars and hydrocarbons provides additional syngas and offers higher carbon utilization of the biomass feedstock.

The objective of this study is to evaluate the effectiveness of transition metal catalysts for the steam reforming of tars and higher hydrocarbons found in gasifier-derived syngas. Catalyst poisoning by the inorganic constituents (e.g., H_2S) and catalyst coking are generally the two main reasons for the deterioration of the catalyst performance during steam reforming of biomass-derived syngas. In a previous report we demonstrated proof-of-concept for a warm syngas clean-up process that is efficient for removing the inorganic constituents (to ppb level) from the biomass-derived syngas prior

* Corresponding authors.
E-mail addresses: vanessa.dagle@pnnl.gov (V.L. Dagle), Robert.Dagle@pnnl.gov (R. Dagle), Roger.Rousseau@pnnl.gov (R. Rousseau).

http://dx.doi.org/10.1016/j.apcatb.2015.11.022
0926-3373/Published by Elsevier B.V.

to the steam reforming unit [3]. Upon sulfur removal catalyst deactivation due to coking can still be problematic. Thus, in this study we evaluate the steam reforming of tars and other hydrocarbons present in sulfur-free syngas. Tar removing catalysts are grouped into mineral (e.g., dolomite, calcite and magnesite) and synthetic catalysts (e.g., alkali metal-based and transition metal-based catalysts). Mineral catalysts are generally not efficient for secondary tar removal since the polycyclic aromatic hydrocarbons remain in the flue gas [5]. Currently, commercial Ni-based catalysts are widely used for steam reforming of biomass-derived tars [2,5,6]. Most studies pertaining to tar removal have focused on Ni-based catalysts primarily because precious metals typically are too expensive to be used in conventional tubular reactors [7]. However, nickel is well known to be prone to deactivation from coke [2,8]. Very few studies have evaluated Group VIII precious metals specifically for tar removal. Tomishige et al. suggested the following activity order for steam reforming of biomass-derived tars when using a CeO_2-SiO_2 support: Rh > Pt > Ni > Pd> Ru [9]. Rh-based catalysts were found to be less susceptible to coking in comparison with other Group VIII metals. Steele et al. also reported a Rh-based catalyst to offer significantly improved catalyst performance when compared to a Ni-based catalyst [10]. Group VIII precious metals are generally well known for their resistance to carbon formation in other steam reforming processes [7,11]. Precious metal catalysts have thus been evaluated for this project specifically for steam reforming the hydrocarbons present in tar-laden biomass gasifier-derived syngas. For more information on tar removal catalysts, readers are directed to excellent reviews by Yung et al. [2], Torres et al. [5], and Dayton [6].

Previously, we showed that the nature of the support (i.e., $MgAl_2O_4$ vs. Al_2O_3) affects significantly the Ir and Rh catalysts stability and coking for methane steam reforming [12]. We found that Ir and Rh metals supported on $MgAl_2O_4$ are more active and coke resistant than their counterparts supported on Al_2O_3. Our computational study has demonstrated that a stronger metal-support interaction exists with the $MgAl_2O_4$ support leading to smaller Ir and Rh metal particles ($\leq\sim$2 nm). These small metal particles activate both water and methane more effectively than the larger metal particles interacting with the Al_2O_3 support which leads to better resistance to coking. For this present work, we have thus focused our research work on $MgAl_2O_4$ supported catalysts. In our preceding studies where extensive computational work coupled with some experimental data were presented, highly dispersed ~1-nm Ir and ~2-nm Rh nanoparticles supported on $MgAl_2O_4$ were shown to be active and stable for methane [12] and benzene [13] steam reforming. This encouraged us to investigate these catalysts under more realistic conditions. This study presents the results of our experimental investigation for the steam reforming of a model biomass-derived syngas (steam reforming of tars) over $MgAl_2O_4$ supported catalysts. The performance of the $MgAl_2O_4$ supported Rh and Ir catalysts is first briefly compared to the one for a commercial Ni-based reforming catalyst and other conventional noble metal (i.e., Ru, Pt, and Pd) catalysts supported on $MgAl_2O_4$. Although the supported Ir and Rh catalysts are significantly more efficient, we show how their stability can be altered under realistic reaction conditions. Beneficial effects have been reported when adding noble metals such as Au to Ni catalysts for other reforming reactions [14]. We have thus designed bimetallic IrNi catalysts supported on $MgAl_2O_4$ and present for the first time their performance for the steam reforming of tars. Our comprehensive investigation demonstrates the potential of IrNi catalysts for steam reforming reactions as improved stability is observed as compared to $MgAl_2O_4$ supported monometallic Ni and Ir catalysts. To complete our experimental investigation, a concise theoretical study is finally shown to provide some insight into the catalyst performance of the bimetallic IrNi catalysts.

2. Experimental and theoretical methods

2.1 Experimental details

2.1.1. Catalysts preparation

A series of supported noble metals catalysts were prepared by incipient wetness impregnation of $MgAl_2O_4$ (Sasol Puralox 30/140), pre-calcined at 500 °C, with solutions of rhodium nitrate (10 wt%), platinum nitrate (13 wt%), ruthenium nitrosyl nitrate (10.19 wt%), palladium nitrate (20 wt%), and iridium acetate (14 wt%) dissolved in deionized water. After impregnation, the catalysts were dried at 110 °C for 8 h and calcined under air at 500 °C for 3 h. The metal loading was 5 wt% for all of the catalysts that are designated as 5%Rh/$MgAl_2O_4$, 5%Pt/$MgAl_2O_4$, 5%Ru/$MgAl_2O_4$, 5%Pd/$MgAl_2O_4$, and 5%Ir/$MgAl_2O_4$.

A series of bimetallic IrNi catalysts were prepared by incipient wetness impregnation of the $MgAl_2O_4$ (Sasol Puralox 30/140) pre-calcined at 500 °C with solutions of nickel nitrate hexahydrate and iridium acetate dissolved in deionized water. After impregnation, the catalysts were dried at 110 °C for 8 h and calcined under air at 500 °C for 3 h. The nickel loading was 15 wt% for all the catalysts, and the Ir loading was between 0 and 5 wt%. The catalysts are designated as *x*%Ir15%Ni/$MgAl_2O_4$ where "*x*" represents the Ir loading except for the catalyst with 0%Ir designated as 15%Ni/$MgAl_2O_4$. A commercial methane steam reforming catalyst obtained from United Catalysts Inc., (C11-9-02, nominal composition: 12%Ni, 88% Al_2O_3 support) also was tested for comparison purposes.

2.1.2. BET surface area

Nitrogen adsorption was measured at 77 K with an automatic adsorptiometer (Micromeritics ASAP 2000). Samples were pretreated at 150 °C for 12 h under vacuum. The surface areas were determined from adsorption values for five relative pressures (P/P_0) ranging from 0.05 to 0.2 using the Brunauer–Emmett–Teller (BET) surface method. The pore volumes were determined from the total amount of N_2 adsorbed between $P/P_0 = 0.05$ and $P/P_0 = 0.98$.

2.1.3. Temperature programmed reduction

Temperature programmed reduction (H_2-TPR) experiments were performed on an automated catalyst characterization unit (Micromeritics Autochem 2910) equipped with a thermal conductivity detector. The catalyst (0.1 g) was loaded in a U-type quartz tube. Then, a 5% H_2/Ar mixture was flowed through the sample starting at 50 °C and ramping up the temperature to 900 °C at a rate of 10 °C/min.

2.1.4. Scanning transmission electron microscopy

Scanning transmission electron microscopy (STEM) measurements were conducted with an FEI Titan 80-300 operated at 300 kV. The FEI Titan is equipped with CEOS GmbH double-hexapole aberration corrector for the probe-forming lens, which allows imaging with ~0.1 nm resolution in STEM mode. The STEM images were acquired on high angle annular dark field (HAADF) with an inner collection angle of 52 mrad. In general, the STEM sample preparation involved mounting powder samples on copper grids covered with lacey carbon support films and then immediately loading them into the STEM airlock to minimize an exposure to atmospheric O_2. STEM images were used to determine average metal particle sizes after reduction at 850 °C or after stability measurements under methane steam reforming reaction conditions. For the samples analyzed after reaction, the term "spent" sample/catalyst is used throughout this manuscript. Approximately 200 particles were counted in determining the average size.

2.1.5. X-ray powder diffraction

X-ray diffraction (XRD) spectra were recorded using a Philips X'pert MPD (Model PW3040/00) diffractometer with copper anode ($K\alpha_1$ = 0.15405 nm) and a scanning rate of 0.002° per second between 2θ = 10–80°. The diffraction patterns were analyzed using Jade 5 (Materials Data Inc., Livermore, CA) and the Powder Diffraction File database (International Center for Diffraction Data, Newtown Square, PA). Ni Particle sizes of the bimetallic IrNi samples were determined from the XRD patterns using the Debye–Sherrer relation ($d = 0.89\lambda/B\cos\theta$, where λ is the wavelength of Cu Kα radiation, B is the calibrated half-width of the peak in radians, and θ is the diffraction angle of a crystal face). The Ni° particle sizes were determined from the peak located at 2θ = 51.95°. The catalysts were reduced at 850 °C for 12 h prior to XRD analysis. For the 5% Ir/$MgAl_2O_4$ and 5% Ir15%Ni/$MgAl_2O_4$ catalysts, the STEM images have indicated that Ir is mainly dispersed as small ($\leq$2 nm) Ir clusters. However, some larger Ir particles also were observed; therefore, we conducted a quantitative phase analysis to determine the ratio between the small Ir clusters and large Ir particles. The analysis was carried out by Rietveld refinement of the XRD patterns using crystal structures from the Inorganic Crystal Structure Database (National Institute of Standards and Technology, MD, and Fachinformationszentrum, Karlsruhe Germany). These refinements used the fundamental parameters approach implemented in Topas (V4.2, Bruker AXS, Germany), with crystallite size modeled by double-Voigt line broadening [15]. Phase quantities are derived from the scale factors used to match the diffraction patterns calculated from each crystal structure to the experimental pattern and are scaled to a total of 100%. The lattice parameters, but not atomic coordinates, were relaxed during refinement to give the best fits.

2.1.6. Total carbon analysis

Total carbon analysis was performed in order to quantify carbon deposition (coke) on the catalyst surfaces after reaction. Total carbon analysis was performed using a Shimadzu TOC-5000A TOC analyzer equipped with a non-dispersive infrared detector. The quantification range of the instrument was 500 ppb–4000 ppm. All samples are analyzed in triplicate and results averaged.

2.1.7. Reactivity

Catalytic activity tests for the steam reforming of methane and tars (i.e., benzene and naphthalene) were conducted in a 1/4-in. outer-diameter (0.18-in. inner-diameter) fixed-bed Inconel reactor. A K-type thermocouple was placed in the reactor to measure the catalyst bed temperature. Heat and mass transfer effects were minimized by using relatively small catalyst particle sizes (i.e., 60–100 mesh), diluting 9 mg of catalyst with 90 mg of α Al_2O_3, and using high linear flow velocities. Experimental results establishing these conditions to predominantly exclude heat and mass transfer effects can be discerned in our previous report [12]. The diluted catalyst was loaded between two layers of quartz wool. A "blank" experiment was conducted using α alumina. For each test, the catalysts were first reduced in situ at 850°C for 12 h, using a 10 mol% H_2/He gas mixture. Then, the gas mixture was introduced into the system using a Brooks mass flow controller (5850E series). As shown in Table 1, the gas mixture feed composition contains 52.6% H_2O, 19.7% H_2, 9.9% CO_2, 9.9% CO, 5.6% methane, 0.95% C_2H_4, 0.95% He, 0.34% benzene, and 0.06% naphthalene unless otherwise indicated. This feed composition was chosen based on a representative gas composition biomass gasifier effluent, although it should be noted that it contains no inorganic purities (e.g., H_2S) and, thus, represents an already purified syngas mixture.

Water was fed into the system using a micro-channel vaporizer and a high-performance liquid chromatography syringe pump (Accuflow Series III). Naphthalene dissolved in benzene was fed to the system using a micro-channel vaporizer and an ISCO syringe pump. Gaseous effluent was analyzed using an Inficon micro-gas chromatography instrument (Model 3000A) equipped with MS-5A, Plot U, Alumina and OV-1 columns and a thermal conductivity detector. Methane and tars conversions were measured over a temperature range (600–850 °C), at atmospheric pressure, and at gas hour space velocities (GHSV) in a 7300–216,000 h^{-1} range (calculated including both diluent and catalyst volume).

Table 1
Model syngas feed composition.

Species	Mol%
H_2	19.7
CO	9.9
CO_2	9.9
CH_4	5.6
C_2H_4	1.0
C_6H_6	3400 ppm[a]
$C_{10}H_8$	600 ppm[a]
H_2O	52.6
He	Balance

[a] Concentration varied for some tests as indicated.

With respect to biomass gasification, the term "tar" refers to a complex mixture of secondary and tertiary aromatic hydrocarbons. Tar has been more rigorously defined as organic contaminants with molecular weights greater than that of benzene [5]. However, benzene is a target for removal as it is a major organic contaminant in biomass-derived syngas [5]. Thus, we have used both benzene and naphthalene in our model feeds. In this paper, we refer to both benzene and/or naphthalene as "tars."

2.2. Theoretical details

Calculations were carried out using spin-polarized density functional theory (DFT) as implemented in the CP2K package [16]. The exchange-correlation energy is accounted for by the generalized-gradient approximation with Perdew–Burke–Ernzerhof functional [17]. The wave functions were expanded in a double-zeta quality Gaussian basis set, and an auxiliary plane-wave basis with a 480-Ry energy cutoff was used in the calculation of the electrostatic energy terms. Core electrons were modeled by scalar relativistic, norm-conserving pseudopotentials [18], and only the Γ-point approximation was employed for Brillouin zone integration. A orthorhombic c(2×3) $MgAl_2O_4$(111) supercell with 15 atomic layers was used to model the spinel oxide support [12]. All periodic slab models include a 20-Å vacuum layer between periodic images in the z direction, and at least 7–8 Å between the supported metal clusters and their periodic images in the x and y directions. To investigate how the structure of the metal clusters may be affected by the support material, we performed ab initio molecular dynamics simulations of ~1 nm diameter metal clusters (Ir_{50}, Ni_{50}, and Ir_5Ni_{45}) supported on a $MgAl_2O_4$(111) surface at T = 1000 K. All ab initio molecular dynamics simulations were performed by sampling the canonical ensemble, employing Nosé–Hoover thermostats [19]. After an initial equilibration phase of 5–10 ps, a well-equilibrated trajectory of at least 10–20 ps at T = 1000 K was collected and analyzed. Methane dissociation was used as the prototypical reaction to evaluate the size effect on activity. Metal clusters (25–50 atoms) were used as models of small particle size catalyst, and metal surfaces such as $p(6 \times 6)$ Ir(111) and Ni(111) were used as models for larger particles.

3. Results and discussion

In our previous work concerning methane steam reforming over $MgAl_2O_4$-supported group VIII metals, we reported that methane turnover at 873 K generally proceeded along the following order of

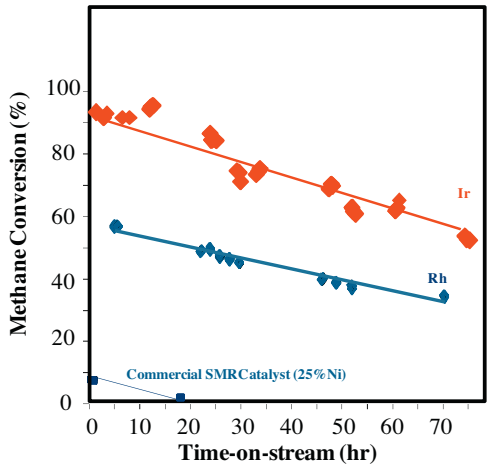

Fig. 1. Stability comparison using model syngas feed containing benzene and naphthalene over 5%Rh/$MgAl_2O_4$ and 5%Ir/$MgAl_2O_4$. Test conditions: T = 850 °C, P = 1 bar, GHSV = 114,000 h^{-1}.

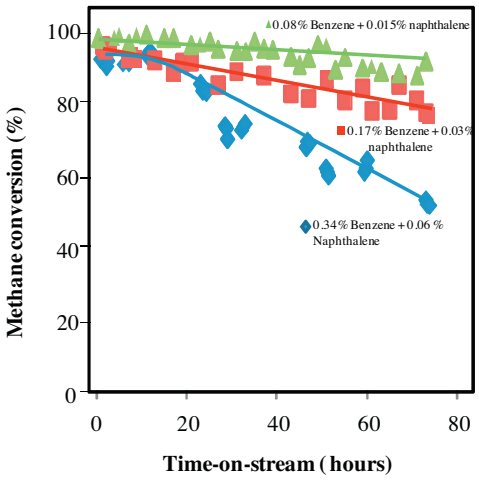

Fig. 2. Effect of tar concentration in the model syngas feed gas over 5%Ir/$MgAl_2O_4$. T = 850 °C, 1 bar, GHSV = 114,000 h^{-1}.

activity: Pd > Ir > Pt∼Rh > Ru > Ni [12]. In the present study, we have examined the stability of these catalysts for the steam reforming of a simulated biomass-derived syngas in the absence of tar (i.e., benzene and naphthalene). The results presented in the supplemental information (Fig. S1–S3, Table S1) show higher methane conversion and better stability for the 5%Ir/$MgAl_2O_4$ and 5%Rh/$MgAl_2O_4$ catalysts. These stability measurements for methane steam reforming suggested that supported Ir and Rh catalysts are preferred noble metal catalysts for steam reforming of tars. For this reason, they have been investigated further.

3.1. Stability comparison of Rh and Ir for steam reforming of methane and tars

In a separate set of experiments, we assessed stability for the 5%Ir/$MgAl_2O_4$ and 5%Rh/$MgAl_2O_4$ catalysts under methane steam reforming conditions in the presence of tars (i.e., benzene and naphthalene). Fig. 1 shows the evolution of methane conversion with TOS for the supported Ir and Rh catalysts as well as for a commercial hydrocarbon steam reforming catalyst (United Catalyst Inc., C11-9-02). The initial methane conversion is 92%, 58%, and 8%, for the 5%Ir/$MgAl_2O_4$, 5%Rh/$MgAl_2O_4$, and commercial Ni catalysts, respectively. As expected, the methane conversion is significantly higher for both supported noble metals. The conversion is higher when using Ir metal that is currently cheaper than Rh metal (although it should be noted that market prices can appreciably vary).

One can also see from Fig. 1 that the 3 catalysts deactivate with TOS. The conversion decreases between TOS = 5–70 h from 92 to 65% and from 58 to 32%, for the 5%Ir/$MgAl_2O_4$ and 5%Rh/$MgAl_2O_4$ catalysts, respectively. The commercial Ni catalyst becomes completely inactive after only 20 h' time on stream. Separate characterization by TEM and total carbon analysis indicates the loss of activity is primarily due to coking of the Ir and Rh catalyst. However for the commercial Ni catalyst, deactivation is due to both sintering and coking. While supported Ni catalysts are conventionally used for hydrocarbon steam reforming, Ni is well known to deactivate due to severe metal particle sintering and carbon deposition, particularly when operating at high temperatures [20]. It is essential to highlight that these experiments were carried out with 0.4% (molar) of tars in the feed stream. The amount of tars added to the feed was intentionally high as compared to the amount of tars in the product gas mixture of a typical gasifier (<0.1 mol% tars) [21].

3.2. Effect of tar concentration in the feed on catalyst stability

The stability of the 5%Ir/$MgAl_2O_4$ catalyst was assessed for the steam reforming of methane and tars (i.e., benzene and naphthalene) for three different tar concentrations. Fig. 2 shows the evolution of methane conversion as a function of the TOS with tar concentrations of 0.4, 0.2, and 0.1% (molar). It can be seen from Fig. 2 that the concentration of tars has a significant impact on catalyst stability. While the conversion decreases from initially 92 to 54% after 70 h with a tar concentration of 0.4%, it decreases only from 95 to 91% with a tar concentration of 0.1%. Hence, under more practical conditions, the loss of activity is relatively low (4% loss in a period of 70 h) for the 5%Ir/$MgAl_2O_4$ catalyst.

3.3. Effect of tar composition on catalyst stability

It is known that catalyst poisoning increases rapidly with the molecular weight and boiling point of the hydrocarbon (tar) feedstock [22,23]. Here we demonstrate how the type of tar, benzene and/or naphthalene, affects stability of the 5%Ir/$MgAl_2O_4$ catalyst for the steam reforming of methane. First tars are not included in the feed, then with just benzene (one C_6-ring aromatic), and finally with both benzene and naphthalene (two C_6-rings aromatic) addition to the feed. The results are shown in Fig. 3. In absence of tars, catalyst deactivation is limited and the conversion decreases only slightly from 95% (TOS = 2 h) to 92% (TOS = 76 h).

When both benzene and naphthalene are added to the gas mixture, there is a significant loss of activity with time. In fact, the conversion decreases from 92% (TOS = 2 h) to 54% (TOS = 76 h). When only benzene is added to the feed, catalyst deactivation is noticeably restrained and the conversion decreases only from 90% (TOS = 2 h) to 80% (TOS = 76 h). Experiments where only naphthalene is added to the feed were not conducted. However, since adding only 0.06% naphthalene to the feed leads to the most noticeable deactivation we can deduce that naphthalene is the main compound responsible for the decrease of activity. These results confirm that the type of tar influences catalyst stability, and illustrates the more pronounced loss of activity from two C_6-ring aromatics than from one C_6-ring aromatic.

3.4. Effect of reaction temperature on catalyst stability

Catalytic steam reforming of tars is typically carried out with supported Ni-based catalysts at temperatures between 600 and 900 °C and preferentially at the higher end [5,23]. Several previous

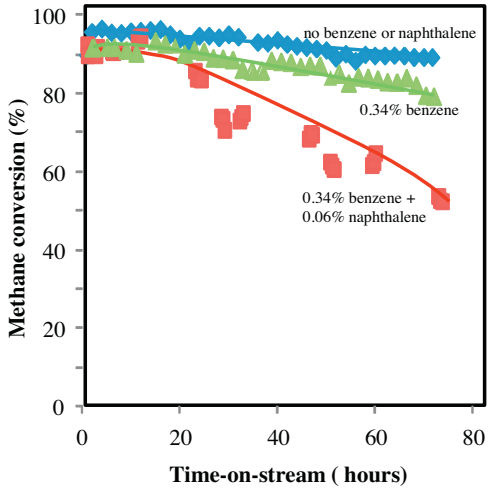

Fig. 3. Effect of the type of tar (benzene, naphthalene) on catalyst stability for the steam reforming of model syngas over 5%Ir/$MgAl_2O_4$. Test conditions: T = 850 °C, P = 1 bar, GHSV = 114,000 h^{-1}.

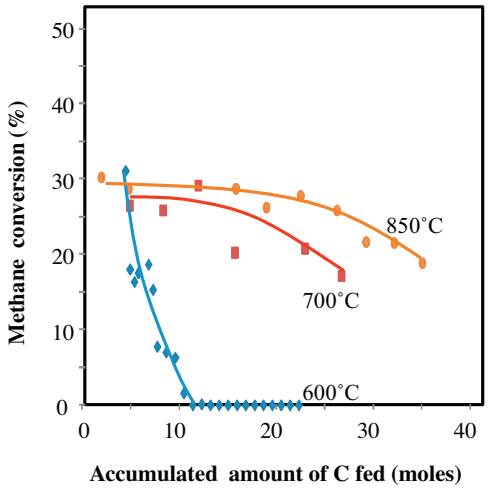

Fig. 4. Effect of reaction temperature on catalyst stability for steam reforming of model syngas containing tar over 5%Ir/$MgAl_2O_4$. Test conditions: T = 600–850 °C, P = 1 bar, GHSV = 7300–216,000 h^{-1}.

studies dedicated to Ni-based catalysts have indicated that carbon formation is prone to increase at lower temperature for steam reforming of hydrocarbons [22–24]. In this work, we examined the stability of the 5%Ir/$MgAl_2O_4$ catalyst for the steam reforming of methane in the presence of tars at 600, 700, and 850 °C. The results are presented in Fig. 4.

For comparison purpose, the GHSV was modified to ensure that the initial conversion would be similar for the three temperatures tested. The results have thus to be presented as a function of the total amount of carbon fed rather than TOS. It is clear from Fig. 4 that catalyst deactivation is higher at the lowest temperature. Indeed, the catalyst is completely deactivated when a total of 10 moles of carbon were fed. For the same amount of carbon fed, the loss of activity is not remarkable at reaction temperatures of 700 and 850 °C. However, when the amount of carbon fed is increased and is over 15 moles, one can see that methane conversion decreases and the loss of activity is more obvious at 700 °C than at 850 °C. The higher deactivation observed at lower temperatures (600–700 °C) is attributed to coking. Since carbon deposition is favored at lower temperatures, the mechanism involved in coke deposition is catalytic and not pyrolytic [23]. At lower temperatures, the coking

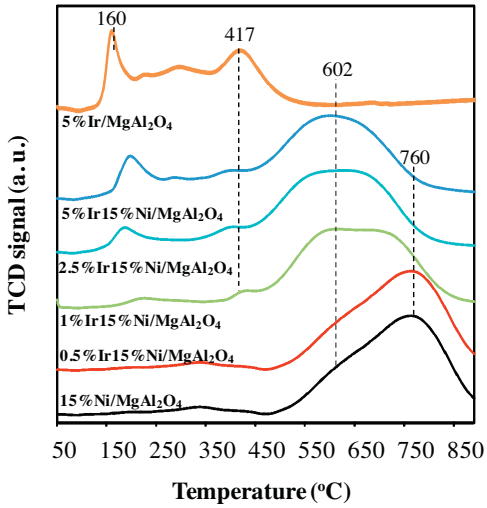

Fig. 5. H_2-TPR profiles for the bimetallic Ir15%Ni/$MgAl_2O_4$ catalysts, and 15% Ni/$MgAl_2O_4$ and 5% Ir/$MgAl_2O_4$ catalysts.

formation rate is higher than the rates of both reforming and carbon gasification reactions and, consequently, higher deactivation is seen. Hence, these results show that operating at higher temperatures (≥850 °C) is preferred to limit catalyst deactivation for steam reforming of methane and tars over the 5%Ir/$MgAl_2O_4$ catalyst.

3.5. Characterization and reactivity of bimetallic IrNi catalysts

Although the 5%Ir/$MgAl_2O_4$ catalyst is considerably more active and stable than the commercial nickel catalyst for steam reforming of methane, deactivation mainly because of coking still occurs, especially when tars are added to the feed. Previous work reports that, for supported nickel catalysts, deactivation by carbon formation can be controlled by modifying Ni° surfaces with a second metal, through alloy formation [25–27]. In addition, it is well known that adding Ir to a Pt/Al_2O_3 steam reforming catalyst diminishes the coke deposit rate and improves stability with time [28]. Supported IrNi catalysts could thus be promising candidates for steam reforming of methane and tars. We have thus synthesized, characterized, and tested several bimetallic IrNi catalysts with 0.5–5% Ir and 15%Ni for steam reforming of methane and tars. Note that the chosen Ni loading is comparable to the one for the commercial Ni catalyst (12%).

3.5.1. Catalysts characterization

Ir and Ni catalysts were analyzed by means of BET surface measurements, H_2-TPR, XRD and TEM to better understand the effect of Ir additive since promoting Ni-based catalyst with Ir is atypical. Table 2 presents the BET surface for the bimetallic IrNi catalysts, the 15%Ni/$MgAl_2O_4$ and 5%Ir/$MgAl_2O_4$ catalysts. One can see that the BET surface of the supported IrNi catalysts is slightly higher than that of the 15%Ni/$MgAl_2O_4$ catalyst (i.e., 86 m^2/g) and lower than that of the 5%Ir/$MgAl_2O_4$ catalyst (i.e., 121.9 m^2/g). However, when the Ir content is between 0.5–5%, the BET surface does not seem to be affected by the amount of Ir promoter.

H_2-TPR experiments were conducted and the profiles are presented Fig. 5. For the 15%Ni/$MgAl_2O_4$ catalyst the main peak is located between 450 and 850 °C with a maximum at 760 °C. The maximum of this peak is shifted toward the lower temperatures when the Ir loading increases and is observed at 602 °C for the 5%Ir15%Ni/$MgAl_2O_4$ catalyst. The results indicate that adding Ir to the 15%Ni/$MgAl_2O_4$ catalyst facilitates the reduction of the NiO species. Note that, for a 10%Ni/Al_2O_3 catalyst, it was similarly reported that adding 0.7% Ir results in a weaker interaction between

Table 2
BET surface area and Ni particle size for the IrNi catalyst series. Ni particles size after reduction at 850 °C, and after steam reforming of model feed gas containing tars (Fig. 8).

Catalyst	BET surface (m^2/g)	Ni particles size (nm)		Metal particles form and identity
		Reduced	Spent	
$15\%Ni/MgAl_2O_4$	86.3	6.6	62.8	Ni particles
$0.5\%Ir15\%Ni/MgAl_2O_4$	94.4	5.6	31.4	Ir single atoms Ir° clusters (≤2 nm) Ir° rich clusters (≤2 nm) containing Ni Ni° rich particles (≥5 nm) containing Ir Ni° particles (≥5 nm)
$1\%Ir15\%Ni/MgAl_2O_4$	93.1	6.6	28.6	
$2.5\%Ir15\%Ni/MgAl_2O_4$	106.4	5.9	22.8	
$5\%Ir15\%Ni/MgAl_2O_4$	99.0	6.6	19.0	Ir single atoms Ir° clusters (≤2 nm) Large Ir° particles (≥30 nm) Ir° rich clusters (≤2 nm) containing Ni Ni° rich particles (≥5 nm) containing Ir Ir Ni intermetallics Ni° particles (≥5 nm)
$5\%Ir/MgAl_2O_4$	121.9	N/A	N/A	Ir single atoms Ir° clusters (≤2 nm) Large Ir° particles (≥30 nm)

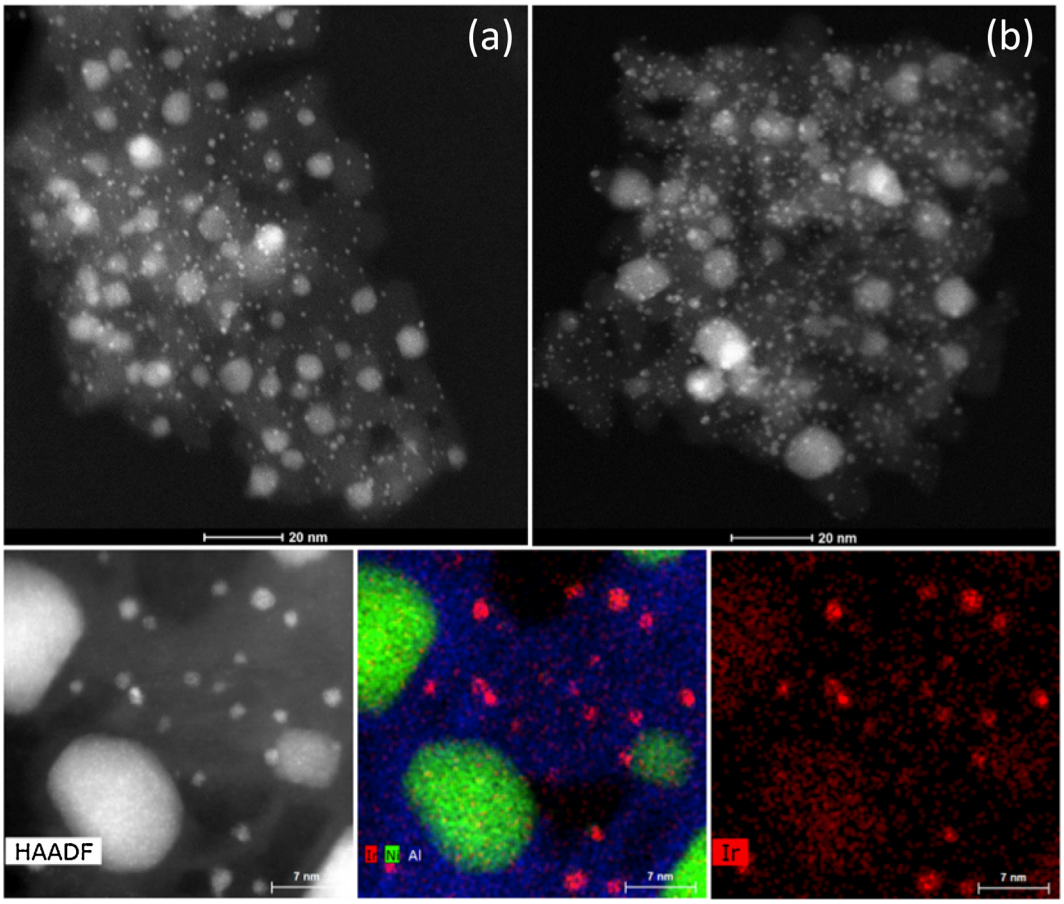

Fig. 6. STEM-HAADF imaging of $2.5\%Ir15\%Ni/MgAl_2O_4$ (a) and $5\%Ir15\%Ni/MgAl_2O_4$ (b) catalysts. The observations show a bimodal distribution of the particles. Based on energy dispersive X-ray spectroscopy (EDS) mapping the larger particles were identified as Ni-rich and small particles were identified as Ir rich.

NiO and the support, thereby contributing to a decrease of the reduction temperature of NiO [29]. For the bimetallic IrNi catalysts with 2.5–5% Ir, two peaks observed at 160–200 °C and 417 °C could result from reduction of bigger and smaller IrO_2 species, respectively [30]. The STEM-HAADF data presented Fig. 6 indicate the presence of both Ir atoms and Ir° clusters that are ≤2 nm in size. The intense peak at 180–200 °C is shifted toward the higher temperatures compared to the H_2-TPR profile of the $5\%Ir/MgAl_2O_4$ (peak located at 160 °C). This result suggests an increase of the reduction temperature of the bigger IrO_2 species by addition of Ni to the $5\%Ir/MgAl_2O_4$ catalyst.

Fig. 7a shows the XRD patterns recorded between $2\theta = 10–80°$ for the supported IrNi, Ni, and Ir catalysts. The Ni° particle size, calculated from the XRD patterns presented in Fig. 7a is comparable and between 5.6 and 6.6 nm for all the catalysts containing nickel. It indicates that the Ni° dispersion is similar for the $15\%Ni/MgAl_2O_4$

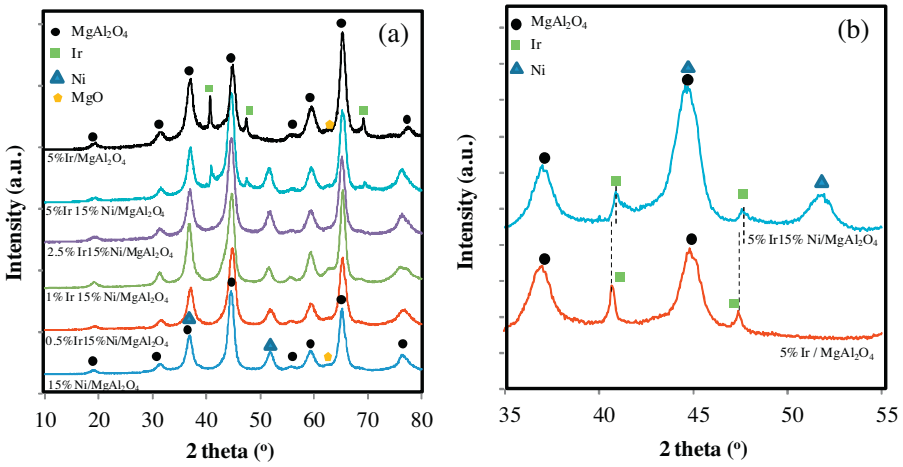

Fig. 7. XRD patterns recorded after reduction at 850 °C, (a) between $2\theta = 10–80°$ for the bimetallic IrNi catalysts, the 15% $Ni/MgAl_2O_4$, catalyst and the 5% $Ir/MgAl_2O_4$ catalyst and (b) between $2\theta = 35–55°$ for the 5%Ir15% $Ni/MgAl_2O_4$ and the 5% $Ir/MgAl_2O_4$ catalysts.

catalysts and the bimetallic IrNi catalysts. The XRD patterns show peaks characteristic of Ir° only for the 5%Ir15%$Ni/MgAl_2O_4$ and the 5%$Ir/MgAl_2O_4$ catalyst. This is due to the presence of a few large Ir° particles as confirmed by the Rietveld refinement of their patterns. Indeed, the 5%$Ir/MgAl_2O_4$ catalyst contains about 91 wt% of ~1 nm Ir° particles and 8.6 wt% of ~36 nm Ir° particles, whereas the 5%Ir15%$Ni/MgAl_2O_4$ contains 94.6 wt% of ~1 nm Ir° particles and 5.4 wt% of ~29 nm Ir° particles. From Fig. 7b, the peaks characteristic of Ir° are observed to be shifted to larger angle for the 5%Ir15%$Ni/MgAl_2O_4$ (e.g., $2\theta = 40.938°$) as compared to the 5%Ir (e.g., $2\theta = 40.717°$). This is indicative of smaller lattice spacing in the Ir° particles for the 5%Ir15%$Ni/MgAl_2O_4$ catalyst, and it is likely due to the presence of IrNi intermetallics. Note that the peak located at $2\theta = 45°$ and attributed to $MgAl_2O_4$ for the 5%$Ir/MgAl_2O_4$ is slightly shifted to lower angle for the 5%Ir15%$Ni/MgAl_2O_4$ catalyst because of overlapping of the peaks characteristic of Ni° and $MgAl_2O_4$. Since the catalysts were calcined at high temperature, the formation of $NiAl_2O_4$ is possible. Both XRD and TEM measurements did not evidence the presence of the $NiAl_2O_4$ phase. However, the presence of a small amount of $NiAl_2O_4$ phase cannot be ruled out since its concentration could be below the detection limit of both techniques.

We then analyzed the microstructure of the bimetallic IrNi catalysts with 0.5–5% Ir by STEM-HAADF and EDS mapping, which is expected to provide morphological, structural, and compositional information. For all bimetallic IrNi catalysts, we find a bimodal particle size distribution, as shown in Fig. 6a and b for 2.5%Ir15%$Ni/MgAl_2O_4$ and 5%Ir15%$Ni/MgAl_2O_4$ catalysts. The HAADF imaging and EDS mapping shown in Fig. 6c–e indicate the presence of (1) Ir atoms, (2) small clusters (≤2 nm) identified as Ir° rich clusters containing a small amount of Ni°, and (3) larger particles (≥5 nm) identified as Ni° rich particles containing a small amount of Ir°. The composition of the large Ni° rich particles was found to vary depending on the nominal composition of the sample. For the catalyst with a nominal composition of 0.5%Ir15%Ni, we identified approximately 1% Ir in the Ni rich particles (i.e., particles with 99% Ni atoms and 1% Ir atoms), while for the 5%Ir15%$Ni/MgAl_2O_4$ catalyst, the composition of Ir increased to approximately 3% (i.e., particles with 97% Ni atoms and 3% Ir atoms). The presence of Ir° within the larger Ni° rich particles also was observed from detailed high-resolution HAADF imaging by observing individual Ir atoms and ~2–3 atoms clusters within the particles. The individual Ir atoms and small Ir° clusters are seen as bright spots within the Ni° rich particles in Fig. S4. Such a strong contrast from single atoms is achieved by the large difference in atomic numbers between Ir and Ni. Another import observation regarding the composition of Ni rich particles was revealed when the Ir concentration is plotted as function of particle size. For any bimetallic IrNi catalyst with 0.5–5% Ir, the Ir concentration within the smaller Ni° rich particles is higher compared to the larger Ni° rich particles. Results from detailed compositional analysis depicting this trend are shown in Fig. S5 in the supplementary information. This finding can be taken as an indication that some of the Ir atoms are distributed on the surface of the Ni° rich particles. In the case of the 5%Ir15%$Ni/MgAl_2O_4$ catalyst, we also identified a small fraction of large Ni particles that have Ir contents way above a few percent, and in these cases, Ir was identified as the main alloying element. As shown in Fig. S6, the density of these larger Ir°-rich particles is however relatively low. These particles correspond to those identified on the XRD patterns as IrNi intermetallics. Note that the larger Ir°-rich particles were not identified for nominal compositional smaller than 5%Ir, which is consisted with XRD analysis. For each catalyst, Table 2 summarizes the metal particles form and identity of the particles and/or clusters. For the catalysts containing Ir, different types of particles were identified, it is thus difficult to estimate the number of active sites.

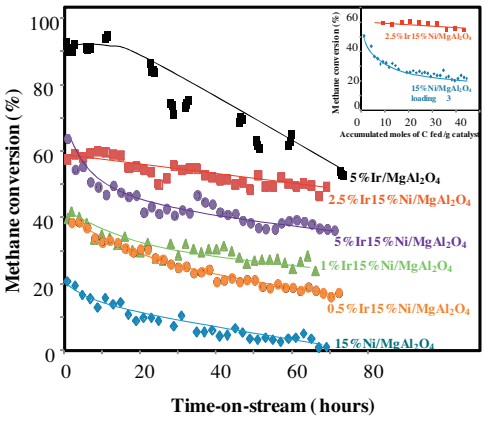

Fig. 8. Comparison of the catalytic performance and stability of the bimetallic IrNi catalysts, and 15% $Ni/MgAl_2O_4$ and 5% $Ir/MgAl_2O_4$ catalysts for steam reforming of model syngas containing tars. Test conditions: $T = 850$ °C, $P = 1$ bar, GHSV = 114,000 h^{-1}. Insert: methane conversion as a function of the amount of carbon fed per gram of catalyst for the 15%$Ni/MgAl_2O_4$ (3 times loading) and the 2.5%Ir15%$Ni/MgAl_2O_4$.

3.5.2. Catalyst performance

The supported IrNi catalysts were tested for steam reforming of methane and tars. The results shown in Fig. 8 are compared with those obtained for the 15%Ni/$MgAl_2O_4$ and 5%Ir/$MgAl_2O_4$ catalysts. Addition of a small amount of Ir (i.e., 0.5 %) to the supported Ni catalyst enhances methane conversion. Indeed, the initial conversion (TOS = 1–2 h) is equal to 40% for the 0.5%Ir15%Ni/$MgAl_2O_4$ and is two times higher than the conversion with the unpromoted Ni catalyst. In addition, the initial methane conversion (i.e., TOS = 1–2 h) increases with the Ir loading and reaches 62% for 5%Ir15%Ni/$MgAl_2O_4$. However, the initial performance of the IrNi catalysts is still lower than the performance of the 5%Ir/$MgAl_2O_4$. In a previous report concerning ammonia decomposition at 300- 450 °C, the better catalytic performance of the bimetallic IrNi/γAl_2O_3 catalysts (10% Ni and 0.5 to 1%Ir) as compared to the monometallic 10%Ni/γAl_2O_3 catalyst was attributed to an increased dispersion of the active nickel and an easier reduction of the NiO species [29]. In the present study, for all the catalysts the H_2-TPR profiles indicate that the NiO species should be totally reduced at temperatures ≥850 °C.

Since the catalysts were reduced in 10%H_2/N_2 at 850 °C for 12 h before reactivity measurements were made, the nickel species for 15%Ni/$MgAl_2O_4$ are expected to be fully reduced. Hence, we do not attribute the increase of activity observed when adding Ir to the 15%Ni/$MgAl_2O_4$ catalyst to a better reduction of the nickel species. In addition, in this study the increased performance of the Ir-promoted Ni catalyst cannot be attributed to better dispersion of Ni. Based on the XRD measurements the Ni dispersion is quite the same for the reduced bimetallic IrNi catalysts and the 15%Ni/$MgAl_2O_4$ catalyst since their Ni° particle size is comparable (i.e., 5.6–6.6 nm). The TEM analysis has indicated that the bimetallic IrNi catalysts present small Ir° rich clusters (≤2 nm) containing Ni° and larger Ni° rich particles (≥5 nm) containing Ir°. Both types of particles can be active species for steam reforming of methane and tars. Thus, it is possible that methane conversion of the bimetallic IrNi catalysts is higher than that of the unpromoted Ni catalysts because the small Ir° rich clusters containing Ni and larger Ni° rich particles containing Ir are more efficient at converting methane and tars than Ni alone. The initial conversion of the 5%Ir15%Ni/$MgAl_2O_4$ catalyst is lower than that of the 5%Ir/$MgAl_2O_4$ catalyst. One possible explanation might be that the Ir° clusters are more active than the small Ir° rich clusters containing Ni and larger Ni° rich particles containing Ir. Another possible hypothesis is that the 5%Ir/$MgAl_2O_4$ catalyst contains a higher number of active sites as compared to the 5%Ir15%Ni/$MgAl_2O_4$ catalyst. We could not verify these hypotheses through experimental measurements because of the complex structure of the 5%Ir15%Ni/$MgAl_2O_4$ catalyst for which different type of particles were identified by TEM (see Table 2). However, the computational investigation presented below indicates that the small Ir_5Ni_{45} cluster supported on spinel and the Ir_3 cluster supported on Ni(111) are more active than the Ir_{50} particles for the formation of carbon monoxide via the route $O + CH \rightarrow CHO^+ \rightarrow CO + H$. This suggests that when normalized per site number higher conversion would be obtained for the 5%Ir15%Ni/$MgAl_2O_4$ catalyst than for the 5%Ir/$MgAl_2O_4$ catalyst. The initial higher conversion observed for 5%Ir/$MgAl_2O_4$ in the present study is thus likely due to a higher number of active sites.

Interestingly, the reactivity measurement presented Fig. 8 also show that adding Ir to the 15%Ni/$MgAl_2O_4$ greatly improves the catalyst stability. By increasing the Ir content up to 2.5%, the loss of activity becomes less and less pronounced. However, for the catalyst promoted with 5% Ir, the loss of activity after 60 h TOS is higher than for the catalyst with 2.5% Ir. There is thus an optimal Ir loading and the 2.5%Ir15%Ni/$MgAl_2O_4$ appears to be the most stable catalyst. This is illustrated by Fig. 9, which shows the ratio of the final/initial conversion for Ir loading between 0 and 5%.

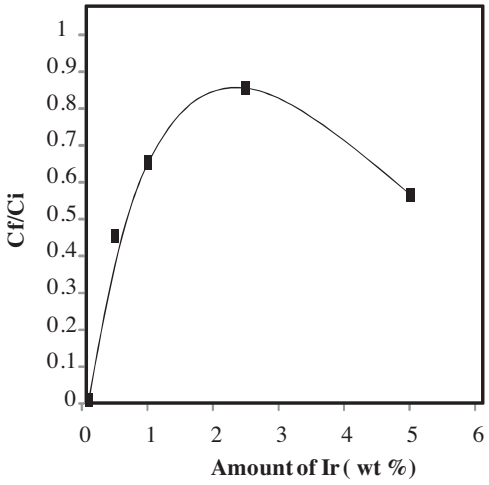

Fig. 9. Ratio of the final conversion (C_f at TOS = 70 h) over initial conversion (C_i at TOS = 1 h) for the 15%Ni/$MgAl_2O_4$ and bimetallic IrNi catalysts.

To provide a better comparison, we evaluated the stability of 15%Ni/$MgAl_2O_4$ and 2.5%Ir15%Ni/$MgAl_2O_4$ at similar initial methane conversion. The results presented in the inset of Fig. 8 indicate that the conversion between TOS = 5 and 45 h decreases from approximately 58 to 52% and from 45 to 22%, respectively, for 2.5%Ir15%Ni/$MgAl_2O_4$ and 15%Ni/$MgAl_2O_4$ catalysts. This confirms the positive impact of the Ir promoter on catalyst stability for the 15%Ni/$MgAl_2O_4$ catalyst. The spent bimetallic Ir15%Ni/$MgAl_2O_4$ and 15%Ni/$MgAl_2O_4$ catalysts were analyzed by XRD, and their patterns were compared to those obtained for the reduced catalysts. Table 2 provides the Ni° particle sizes determined from the XRD patterns of the spent samples. As explained earlier, the Ni° particle size is quite the same for the reduced catalysts. For all the spent catalysts, the Ni° particles size is above 18 nm and is bigger than that for the reduced catalysts indicating that Ni° particles sinter during reaction. Interestingly, for all the spent samples promoted with Ir, the Ni° particle size is notably smaller than for the 15%Ni/$MgAl_2O_4$. For instance, the Ni particle size is equal to 62.8 nm for 15%Ni/$MgAl_2O_4$ and only 31.4 nm for 0.5%Ir15%Ni/$MgAl_2O_4$. In addition, the size of the Ni° particles decreases from 31.4 to 19 nm when the Ir content increases from 0.5 to 5%. These results signify that, Ir can decrease the sintering of the Ni° particles during reaction. Consequently, the better stability of the bimetallic IrNi catalysts compared to the 15% Ni/$MgAl_2O_4$ is in part due to better resistance to sintering during reaction. There was insufficient spent sample for total carbon analysis but the coke formation rate can be anticipated to be less for the bimetallic IrNi catalysts than for 15%Ni/$MgAl_2O_4$ because the Ir additive is known for reducing the coke deposit rate [28]. Another major finding from this study is that the 5% Ir/$MgAl_2O_4$ catalyst suffers from a more rapid deactivation when compared to the 5%Ir15%Ni/$MgAl_2O_4$ catalyst. This is somehow quite surprising since noble metals are typically employed over Ni for their higher resistance to coking. Ir° does not sinter significantly for methane steam reforming (Table S1). On the contrary, sintering of the Ni particles for the 5%Ir15%Ni/$MgAl_2O_4$ catalyst is pronounced when steam reforming both methane and tars. Therefore, we do not believe sintering is responsible for the higher deactivation rate of the 5%Ir/$MgAl_2O_4$ catalyst compared to 5%Ir15%Ni/$MgAl_2O_4$ catalyst. One possible explanation is that coking is less pronounced for the 5%Ir15%Ni/$MgAl_2O_4$ catalyst. Again, this could not be verified experimentally since there was not sufficient amount of spent samples for total carbon analysis. In our

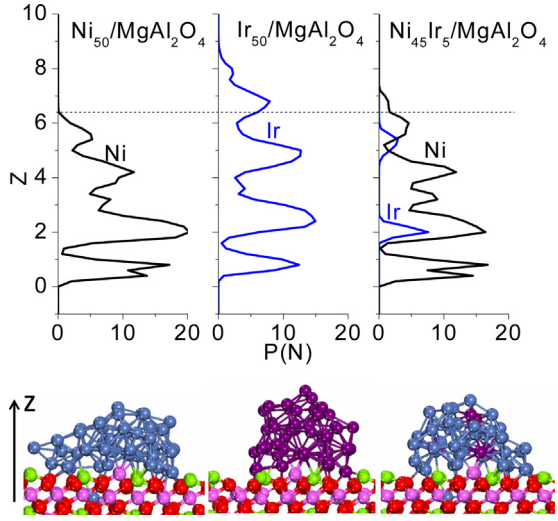

Fig. 10. Simulated equilibrium structures of Ni_{50}, Ir_{50} and Ir_5Ni_{45} clusters on $MgAl_2O_4$ (111) support, and the corresponding distribution densities of metal atoms along the Z direction.

previous work [12], we determined the tendency of the Ir clusters to form coke (i.e., carbon) via DFT calculations of the energetics for methane dissociation. A similar approach was used in the present study and the molecular simulations are presented in the next section.

3.6. Molecular simulations

The theoretical modeling study focused on developing an understanding of (1) the nature of the structure of the IrNi alloy particles, in particular the surface enrichment of Ir, (2) the relative resistance to coking of the small Ir-rich and large Ni-rich particles, and (3) the activity toward reforming of both types of particles. In a previous report, we examined similar issues for small and large Ir and Rh particles supported on $MgAl_2O_4$ and Al_2O_3 [12].

In the current study, we consider models of Ni_{50}, Ir_{50} and Ir_5Ni_{45} on the $MgAl_2O_4$ (111) surface. Note that Ir_5Ni_{50} corresponds to a cluster with 5 Ir atoms and 50 Ni atoms and a Ir/Ni mass ratio equal to 1/3 equivalent to the mass ratio of 5%Ir15%Ni/$MgAl_2O_4$. Structures were prepared by ab initio molecular dynamics first equilibrated at $T = 1000$ K, and subsequently quenched $T = 0$K. The optimized structures are shown in Fig. 10 along with the distribution of the atoms in the direction along the surface normal.

In comparing the structure of Ni_{50} and Ir_{50}, it has been found that Ni_{50} wets the surface appreciably, with an average of 24 direct Ni-O contacts and leaving ~10 Ni atoms at the interface in a partially positively charged state. In contrast, the Ir_{50} particle shows fewer (~17) direct Ir-O contacts with only about 6 Ir atoms at the interface. This result is consistent with stronger Ni–O interactions at the cluster oxide interface, resulting in an appreciably flatter Ni particle, while the Ir_{50} cluster retains a more spherical shape; see Fig. S7 for further discussion. Although the gas-phase Ir_5Ni_{45} cluster is a well-mixed alloy (see Fig. S8), deposition of the cluster on the spinel surface results in a binding pattern consistent with that of Ni_{50}; approximately 23 direct Ni—O bonds with the ~10 Ni atoms at the interface: see Table S2 and Fig. S9. Notably, Ir is completely excluded from the interface area, so that three Ir atoms are pushed up and reside on the outer surface of the Ir_5Ni_{45} particle. In fact, we observed both isolated Ir atoms as well as an Ir_2 dimer on the cluster surface, which is consistent with the TEM observation of single atoms and small clusters enriching the surface of the Ni particles. The Ir atoms in the mixed alloy cluster also exhibit an enhancement of negative charge greater than those seen

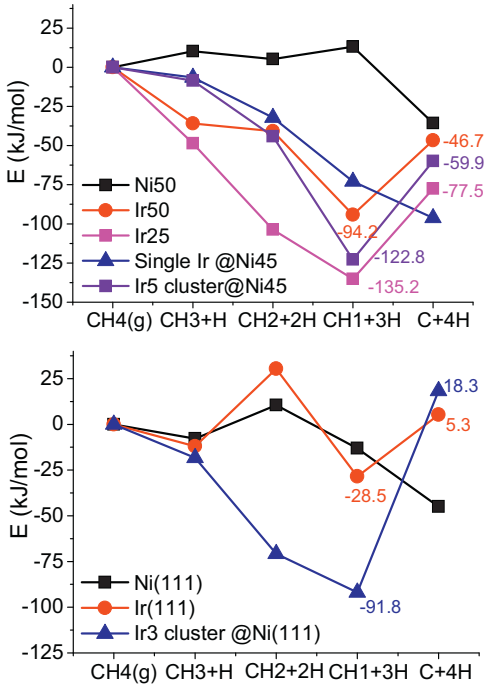

Fig. 11. Binding energies for the intermediates during methane dissociation (KJ/mol). The energy for methane in the gas phase is selected as the reference. (a) Ni_{50}, Ir_{50}, Ir_{25}, and Ir_5Ni_{45} cluster model on spinel $MgAl_2O_4$ support. (b) Ni(111), Ir(111), and Ir_3@Ni(111) surface model.

in the Ir_{50} cluster. Specifically, Bader population analysis (see Table S3) indicated that the average charge accumulation of Ir atoms in Ir_{50} is about $-0.05e^-$, whereas those in Ir_5Ni_{45} show an average of $-0.78e^-$. This enhancement results from a transfer of charge from the Ni atoms, which are more positively charged at the interface, see SI. These results indicate that the formation of the strong Ni–O interactions at the metal/spinel interface lead to a segregation of Ir atoms at the surface of the IrNi particles. These Ir atoms provide a locus where negative charge can accumulate and create a stronger reducing agent compared to the Ir_{50} cluster.

To investigate the ramifications of these observations on the catalytic performance, we consider the propensity of these clusters to form coke (carbon). Similar to our previous study [12], we investigated the energetics of the decomposition of the simple hydrocarbon CH_4 to $CH_3 + H$, $CH_2 + 2H$, $CH + 3H$, and $C + 4H$. Selected optimized configurations are presented in section S3 of SI. The relative energetics of the last reaction $CH + 3H \rightarrow C + 4H$, $\Delta E_{CH/C}$, is taken as a measure of the propensity of the cluster to form coke. In Fig. 11, we show that both Ni(111) and Ni_{50} supported on spinel highly favor the formation of coke ($\Delta E_{CH/C} < 0$), which is consistent with the observation that Ni particles tend to coke. Also shown by our previous study, smaller Ir clusters, stabilized on the spinel surface, are more resistant to coking such that Ir(111) ($\Delta E_{CH/C} = 34$ kJ/mol) < Ir_{50} ($\Delta E_{CH/C} = 48$ kJ/mol) < Ir_{25} ($\Delta E_{CH/C} = 58$ kJ/mol) [12]. In this context, it is interesting to note that the Ir in IrNi alloy particles is also coke resistant, except in the case of the isolated Ir single atoms. For instance, the $\Delta E_{CH/C}$ is equal to 63 kJ/mol when all Ir atoms agglomerate onto the surface of the Ir_5Ni_{45} particle. Conversely, isolated Ir atoms on the Ir_5Ni_{45} particle favor coke formation and $\Delta E_{CH/C} < 0$ kJ/mol, in this case the neighboring Ni sites dominate reactivity. Furthermore, this same observation carries over to larger particles such that an isolated Ir site on a Ni(111) surface behaves essentially like Ni(111) with respect to coke formation ($\Delta E_{CH/C} < 0$ kJ/mol), while a small Ir cluster (Ir_3) on the same surface shows enhanced coke resistance ($\Delta E_{CH/C} = 110$ kJ/mol).

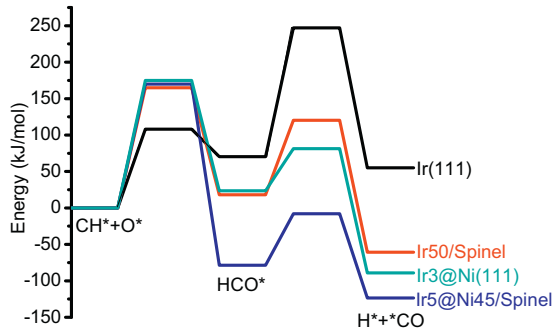

Fig. 12. Reaction energy profile for carbon monoxide formation via the route $O + CH \rightarrow CHO^{+} \rightarrow CO + H$ on selected Ir clusters and bulk (111) surface.

These observations correlate well with the results of our stability tests. Small Ir clusters show enhanced resistance to coke during reforming relative to Ni alone, but the greatest resistance to coke is observed when small Ir clusters supported on Ni particles. Based on these arguments, we interpret the enhanced stability observed as the weight loading of Ir increases from 0 to 2.5%, as resulting from the enhanced population of small Ir clusters on the surface of the larger Ni particles. As the Ir weight loading increases from 2.5 to 5%, a larger fraction of the Ir is present in ≤2 nm Ir clusters on the spinel, which themselves are less coke resistant than the small clusters on the surface of the Ni particles.

Our simple model supports the observation that coke resistance is a function of Ir loading. We now consider whether or not the small Ir clusters supported on the larger Ni particles are active toward reforming. As pointed out in our previous work on methane steam reforming on small Ir clusters [12], the lowest energy route for reforming proceeds via the decomposition of water to O atoms (favorable on 1-nm sized Ir), which can combine with adsorbed CH: $O + CH \rightarrow H + CO$. The energy profile for this reaction is shown in Fig. 12 for selected Ir particles. Consistent with our previous report, this route is uphill in energy $\Delta E_{CHO} = 55$ kJ/mol with an overall reaction barrier of $\Delta E^{*}_{CHO} = 247$ kJ/mol on Ir(111). On Ir_{50}, a favorable $\Delta E_{CHO} = -60$ kJ/mol is determined, with an overall lower energy barrier ΔE^{*}_{CHO} of 170 kJ/mol. Both the small Ir_5Ni_{45} cluster supported on spinel and the Ir_3 cluster supported on Ni(111) show a low energy barriers for this reaction channel ($\Delta E^{*}_{CHO} = 173$–181 kJ/mol) just as the Ir_{50} cluster does but also enhanced energetic preference for the products ($\Delta E_{CHO} = -89$–123 kJ/mol), which is indicative of higher activity toward this reaction than the 1 nm Ir_{50} particle. Similar conclusions regarding the role of Ir sites on alloyed nanoparticles in the favorable coupling toward HCO formation were also drawn from studies of syngas conversion to C_2^{+} oxygenates [31].

Taken together, our results suggest that the exclusion of Ir from the Ni/oxide interface results in electron-rich Ir atoms and small clusters at the surface of larger Ni particles. These unique reactivity sites show enhanced resistance to coke formation, as well as enhanced activity toward carbon monoxide production. This indicates that small clusters on the order of a few Ir atoms supported on top of the larger Ni particles are expected to be more active and coke resistant than Ni or Ir alone. Hence, the higher initial conversion observed experimentally for 5%Ir/$MgAl_2O_4$ as compared to 5%Ir15%Ni/$MgAl_2O_4$ is likely to be due to its higher number of active sites.

4. Conclusions

In the present study, we have demonstrated that, because of higher stability, Ir/$MgAl_2O_4$ is the most promising catalyst among $MgAl_2O_4$-supported Pd, Pt, Ru, and Ni metals for steam reforming of methane and tars. Ir is more attractive than Rh because of its higher catalytic activity. On a turnover basis, Ir is more active for methane steam reforming and also offers superior metal dispersion when supported on $MgAl_2O_4$. For a 5% Ir/$MgAl_2O_4$ catalyst, we have demonstrated that the loss of activity resulting from carbon formation is controlled by the type and concentration of tar in the feed gas and that it can be minimized at a high reaction temperature (i.e., 850 °C). A major finding is that bimetallic IrNi catalysts are more stable than 15%Ni/$MgAl_2O_4$ and 5%Ir/$MgAl_2O_4$ catalysts for Ir loading between 1 and 5 wt.%. Minimal loss of activity for steam reforming of methane and tars was observed for a catalyst with 2.5%Ir and 15%Ni. STEM-HAADF imaging and EDS mapping reveals the presence of individual Ir atoms, and bimetallic particles comprising both Ir and Ni; small (≤2 nm) Ir°-rich clusters, and larger (≥5 nm) Ni°-rich particles. Theoretical calculations suggest that small Ir (~Ir_3–Ir_5) on the surface of larger Ni-rich particles result in electron-rich Ir sites. These sites lead to enhancement of both durability and activity for steam reforming relative to Ni or Ir alone. A superior activity is thus expected for the bimetallic IrNi catalyst as compared to the monometallic Ir and Ni catalysts when normalized per site number.

Acknowledgements

This work was financially supported by the United States Department of Energy (DOE)'s Bioenergy Technologies Office (BETO) and performed at the Pacific Northwest National Laboratory (PNNL). PNNL is a multi-program national laboratory operated for DOE by Battelle Memorial Institute. Computing time and advanced catalyst characterization use was granted by a user proposal at the William R. Wiley Environmental Molecular Sciences Laboratory (EMSL). EMSL is a national scientific user facility sponsored by the Department of Energy's Office of Biological and Environmental Research and located at PNNL. The authors would like to thank Cary Counts of PNNL for help with technical editing of this manuscript. Finally, the authors would also like to thank and dedicate this paper to Mark Gerber who recently retired from PNNL. Mark had a long history of leading BETO-funded PNNL activities in the area of gasification, syngas cleanup, and syngas conversion. Mark was also instrumental in integrating experimental and theoretical catalysis activities pertaining to mixed alcohol synthesis in addition to syngas cleanup research.

Appendix A. Supplementary data

Supplementary data associated with this article can be found, in the online version, at http://dx.doi.org/10.1016/j.apcatb.2015.11.022.

References

[1] G.W. Huber, S. Iborra, A. Corma, Synthesis of transportation fuels from biomass: chemistry, catalysts, and engineering, Chem. Rev. 106 (2006) 4044–4098.
[2] M.M. Yung, S. Cheah, K. Magrini-Bair, J.N. Kuhn, Transformation of sulfur species during steam/air regeneration on a Ni biomass conditioning catalyst, ACS Catal. 2 (2012) 1363–1367.
[3] C.J. Howard, R.A. Dagle, V.M. Lebarbier, J.E. Rainbolt, L.Y. Li, D.L. King, Progress toward biomass and coal-derived syngas warm cleanup: proof-of-concept process demonstration of multicontaminant removal for biomass application, Ind. Eng. Chem. Res. 52 (2013) 8125–8138.
[4] L. Devi, K.J. Ptasinski, F.J.J.G. Janssen, A review of the primary measures for tar elimination in biomass gasification processes, Biomass Bioenergy 24 (2003) 125–140.
[5] W. Torres, S. Oansare, J. Goodwin, Hot gas removal of tars, ammonia, and hydrogen sulfide from biomass gasification GAs, Catal. Rev. 49 (2007) 407–456.
[6] D. Datyon, A Review of the Literature on Catalytic Biomass Tar Destruction, National Renewable Energy Laboratory, 2002.

[7] G. Jones, J.G. Jakobsen, S.S. Shim, J. Kleis, M.P. Andersson, J. Rossmeisl, F. Abild-Pedersen, T. Bligaard, S. Helveg, B. Hinnemann, J.R. Rostrup-Nielsen, I. Chorkendorff, J. Sehested, J. Norskov, First principle calculations and experimental insight into methane steam reforming over transition metal catalysts, J. Catal. 259 (2008) 147–160.
[8] E.G. Baker, L.K. Mudge, M.D. Brown, Steam gasification of biomass with nickel secondary catalysts, Ind. Eng. Chem. Res. 26 (1987) 1335–1339.
[9] K. Tomishige, T. Miyazawa, M. Asadullah, S. Ito, K. Kunimori, Catalyst performance in reforming of tar derived from biomass over noble metal catalysts, Green Chem. 5 (2003) 399–403.
[10] A.M. Steele, S. Poulston, K. Magrini-Bair, W. Jablonski, Catalytic syngas purification from model biomass gasification streams, Catal. Today 214 (2013) 74–81.
[11] J.R. Rostrup-Nielsen, J.-H.B. Hansen, CO_2-reforming of methane over transition metals, J. Catal. 144 (1993) 38–49.
[12] D. Mei, V.-A. Glezakou, V. Lebarbier, L. Kovarik, H. Wan, K.O. Albrecht, M. Gerber, R. Rousseau, R.A. Dagle, Highly active and stable MgAl2O4-supported Rh and Ir catalysts for methane steam reforming: a combined experimental and theoretical study, J. Catal. 316 (2014) 11–23.
[13] D.H. Mei, V.M. Lebarbier, R. Rousseau, V.A. Glezakou, K.O. Albrecht, L. Kovarik, M. Flake, R.A. Dagle, Comparative investigation of benzene steam reforming over spinel supported Rh and Ir catalysts, ACS Catal. 3 (2013) 1133–1143.
[14] D.L. Li, Y. Nakagawa, K. Tomishige, Methane reforming to synthesis gas over Ni catalysts modified with noble metals, Appl. Catal. A: Gen. 408 (2011) 1–24.
[15] D. Balzar, Voigt-function model in diffraction line-broadening analysis, in: R.L. Snyder, H.J. Bunge, J. Fiala (Eds.), Microstructure Analysis from Diffraction, Oxford University Press, International Union of Crystallography, New York, 1999, pp. 94–123.
[16] CP2K is a program to perform atomistic and molecular simulations of solid state, liquid, molecular, and biological systems. It provides a general framework for different methods such as e.g., density functional theory (DFT) using a mixed Gaussian and plane waves approach (GPW) and classical pair and many-body potentials.
[17] J.P. Perdew, K. Burke, M. Ernzerhof, Generalized gradient approximation made simple, Phys. Rev. Lett. 77 (1996) 3865–3868.
[18] S. Goedecker, M. Teter, J. Hutter, Separable dual-space Gaussian pseudopotentials, Phys. Rev. B 54 (1996) 1703.
[19] S. Nosé, A unified formulation of the constant temperature molecular dynamics methods, J. Chem. Phys. 81 (1984) 511–519.
[20] J. Rostrop-Nielsen, Steam Reforming Catalysts, Danish Technical Press Inc, Copenhagen, 1975.
[21] R.M. Baldwin, K.A. Magrini-Bair, M.R. Nimlos, P. Pepiot, B.S. Donohoe, J.E. Hensley, S.D. Phillips, Current research on thermochemical conversion of biomass at the National Renewable Energy Laboratory, Appl. Catal. B: Environ. 115–116 (2012) 320–329.
[22] F. Moseley, R.W. Stephens, K.D. Stewart, J. Wood, The poisoning of a steam hydrocarbon gasification catalyst, J. Catal. 24 (1972) 18–39.
[23] R. Coll, J. Salvadó, X. Farriol, D. Montané, Steam reforming model compounds of biomass gasification tars: conversion at different operating conditions and tendency towards coke formation, Fuel Process. Technol. 74 (2001) 19–31.
[24] T. Furusawa, K. Saito, Y. Kori, Y. Miura, M. Sato, N. Suzuki, Steam reforming of naphthalene/benzene with various types of Pt- and Ni-based catalysts for hydrogen production, Fuel 103 (2013) 111–121.
[25] D.L. Trimm, Catalysts for the control of coking during steam reforming, Catal. Today 49 (1999) 3–10.
[26] H. Wu, V. La Parola, G. Pantaleo, F. Puleo, A. Venezia, L. Liotta, Ni-based catalysts for low temperature methane steam reforming: recent results on Ni-Au and comparison with other bi-metallic systems, Catalysts 3 (2015) 563–583.
[27] Y.-H. Chin, D.L. King, H.-S. Roh, Y. Wang, S.M. Heald, Structure and reactivity investigations on supported bimetallic AuNi catalysts used for hydrocarbon steam reforming, J. Catal. 244 (2006) 153–162.
[28] J. Barbier, B. Delmon, G.F. Froment, Coking of reforming catalysts, in: Studies in Surface Science and Catalysis, Elsevier, 1987, 2015, pp. 1–19.
[29] X. Han, W. Chu, P. Ni, S.-z. Luo, T. Zhang, Promoting effects of iridium on nickel based catalyst in ammonia decomposition, J. Fuel Chem. Technol. 35 (2007) 691–695.
[30] O. Hernández-Cristóbal, G. Díaz, A. Gómez-Cortés, Effect of the reduction temperature on the activity and selectivity of titania-supported iridium nanoparticles for methylcyclopentane reaction, Ind. Eng. Chem. Res. 53 (2014) 10097–10104.
[31] V.-A. Glezakou, J. Jaffe, R. Rousseau, D. Mei, S. Kathmann, K. Albrecht, M. Gray, M. Gerber, The role of Ir in ternary Rh-based catalysts for syngas conversion to C_2^+ oxygenates, Top. Catal. 55 (2012) 595–600.